Holographic Transmitarray Antenna with linear Polarization in X band

Mahdi Salehi (mahdi_salehi@elec.iust.ac.ir)
Iran University of Science and Technology https://orcid.org/0000-0003-1182-1608
Homayoon Oraizi
Iran University of Science and Technology

Research Article

Keywords: Holographic Transmitarray, Metasurface, Artificial Impedance Surface, Wideband, Transmission Impedance Surface

Posted Date: April 27th, 2021

DOI: https://doi.org/10.21203/rs.3.rs-468556/v1

Holographic Transmitarray Antenna with linear Polarization in X band

Mahdi Salehi[1,*] **and Homayoon Oraizi**[2]

[1]Iran University of Science and Technology, Electrical Engineering, Tehran, 16846-13114, Iran
[2]Iran University of Science and Technology, Electrical Engineering, Tehran, 16846-13114, Iran
[*]mahdi_salehi@elec.iust.ac.ir

ABSTRACT

In this paper, we present the design and demonstration of transmitarray antennas (TAs) based on the holographic technique for the first time. According to the holographic theory, the amplitudes and phases of electromagnetic waves can be recorded on a surface, and then they can be reconstructed independently. This concept is used to design single-beam and multi-beam linearly polarized holographic TAs without using any iterative optimization algorithms. Initially, a transmission impedance surface is analyzed and compared with the reflection one. Then, interferograms associated with the scalar admittance distribution are defined according to the number and direction of the radiation beams. After that, a transmission metasurface of dimensions equal to $0.26\lambda_0$ is hired to design holographic TAs at 12 GHz. Several examples are provided to support the method. In the end, a linearly polarized circular aperture wideband holographic transmitarray antenna with a radius of 13.3 cm has been manufactured and tested. The antenna achieves 12.5% (11.4-12.9 GHz) 1-dB gain bandwidth and 23.8 dB maximum gain, leading to 21.46% aperture efficiency.

Introduction

Transmitarrays have attracted much interest in recent years because of their inherent advantages such as high gain, high radiation efficiency, lightweight, low profile, and simple manufacturing procedure, making them the right candidate for satellite communication, microwave imaging system, and radar applications. A transmitarray is illuminated through space feeding, so compared with the phased array, it does not experience the insertion loss of the feeding network at high frequency. Besides, as a transmitarray is illuminated directly from the back of the aperture, it does not experience the blockage losses expected with reflectarray antennas. The idea of holographic antenna was first published in 1969 by P.checcacci, V. Russo and A.M. Scheggi[1]. Technological developments in PCB and CNC machining have encouraged researchers to improve the idea. Up to now, several holographic antennas (holographic leaky wave antennas and holographic reflectarray antennas) have been designed. In[2], two holographic reflectarray antennas with linear and circular polarizations are proposed. The linearly polarized antenna achieves 25% aperture efficiency, and the circularly polarized antenna achieves 15.57% aperture efficiency. In[3], a multi-beam linearly polarized holographic reflectarray antenna is proposed. It achieves 22.2% 1-dB gain bandwidth and 53.09% aperture efficiency for dual beam radiating. In[4], a circular polarized holographic reflectarray antenna is proposed. The antenna can produce multiple beams with independent circular polarizations. It achieves 19.23% 1-dB gain bandwidth and 45.8% aperture efficiency. In[5], a holographic reflectarray with the capability of producing shaped electromagnetic waves is proposed. The antenna can produce multiple beams with arbitrary shapes. In [6-10], holographic leaky wave antennas are proposed.

According to the authors' knowledge, research into the holographic antenna concept has been limited to reflectarray and leaky wave antennas. Therefore, a detailed study of designing transmitarrays based on the holographic technique is presented here for the first time. This technique makes the TA antenna design process easy and improves its performance, such as radiation efficiency, operational bandwidth, and cross-pol level, comparing with the only-phase technique. As there are differences between the impedance (admittance) characteristic of a transmission and reflection surface, a new method based on the holographic technique is proposed. In order to validate the method, several examples, including single and dual-beam holographic TA, are provided. Finally, a holographic TA is manufactured and tested, obtaining close agreement with simulation results. This paper is organized as follows: Section 2 describes the basics of the holographic theory in the microwave regime. Section 3 analyses the impedance surface for both the reflection and transmission states. Section 4 explains the design procedure of the holographic transmitarray antennas. Section 5 presents the design of the unit cell with simulation results. Section 6 provides examples to validate the design procedure proposed in section 4. All examples are simulated using the CST Studio Suite software, and section 8 discusses the measurement and simulation results. Finally, section 9 presents the conclusion of this study.

1 Basic concepts of the Holographic Technique

Holography is a two steps technique. In the first step, the interference pattern of the object wave (ψ_{obj}) and the reference wave (ψ_{ref}) is calculated, recording necessary information (amplitude and phase) for reconstructing ψ_{obj} . In the second step, the interference pattern is multiplied by ψ_{ref} to reconstruct the object wave. This technique is developed in Eq.(1) to Eq.(3)[11].

$$I = \left|\psi_{ref} + \psi_{obj}\right|^2 \tag{1}$$

$$\psi_{trans} = I \times \psi_{sec} \tag{2}$$

$$\psi_{trans} = \left|\psi_{ref}\right|^2 \psi_{ref} + \left|\psi_{obj}\right|^2 \psi_{ref} + \psi_{obj}^{*} \psi_{ref} \psi_{ref} + \psi_{ref} \left|\psi_{ref}\right|^2 \tag{3}$$

Although four waves are generated in Eq.(3), the first three waves are not expected to exist in the visible region. The last term represents the object wave $\left(\psi_{obj}\left|\psi_{ref}\right|^2\right)$. After doing a few calculations, Eq.(4) is obtained from Eq.(3). According to Eq.(4), the holographic interference pattern is purely amplitude while it contains the phase information of the interfered waves[11].This equation represents the mathematical hologram, so the problem is with the practical realization of the hologram. In[10], the utilization of artificial impedance surfaces with modulated dimensions is proposed to solve this problem. Prior to employing the artificial impedance surfaces, it is vital to provide a mathematical relation between the interference pattern and the impedance surface. This is done by defining Eq.(5)[4]:

$$I = \left|\psi_{ref}^2 + \psi_{obj}^2 + 2\Re\left(\psi_{obj}\psi_{ref}\right)\right| \tag{4}$$

$$Z(x,y)|Y(x,y) = j\left(X + M\Re\left(\psi_{obj}\psi_{ref}^{*}\right)\right) \tag{5}$$

where X and M are arbitrary average impedance (admittance) value and arbitrary modulation depth, respectively. These values must be assigned so that the impedance (admittance) distribution of the hologram can be correctly implemented by the unit cell. After sampling the mathematical hologram (described by Eq.(5)), the usable impedance (admittance) distribution is obtained, making the realization of the hologram possible in the form of an array of quasi-periodic unit cells with variable patch size. The cell's patch size is determined to meet the local impedance (admittance) value of the hologram surface. Also, its dimensions (sampling rate) are determined to satisfy the Nyquist rate.

Transmission and Reflection Impedance surfaces

An impedance surface reflects and transmits waves simultaneously with different coefficients. To study the coefficients in more depth, an impedance sheet with a constant resistance of 20 ohms, and variable reactance values is simulated, as a unit cell, using the ANSYS HFSS software. Master/Slave boundaries are forced on the four sides of the unit cell to simulate an infinite array of sheets. The reflection and transmission magnitudes are shown in Fig.1. As seen in the figure, the transmission magnitude increases by increasing the absolute value of the surface reactance (e.g., the transmission magnitude increases from almost -30 dB to -10.52 dB, as the surface reactance increases from 0 to 60 ohms). By increasing the absolute value of reactance to 360 ohms, the transmission magnitude curve jumps over -1 dB level. In other words, the sheet starts changing its reaction to the electromagnetic waves from reflection to transmission at 360 ohms. This is a critical difference between RA unit cells and TA unit cells, which necessitates applying a method different from what has been proposed in [2-5]. For more clarification, a lossless transmission unit cell is examined. The reactance values of the lossless unit cell as a function of the transmission phase are shown in Fig.2. The reactance values repeat when the transmission phase varies from 0^0 to 180^0 and from -180^0 to 0^0. Therefore, it is required for the unit cell to provide only 180^0 phase range to cover all possible reactance values. However, if the goal is to design a TA based on the only-phase technique, the applied unit cell should provide 360^0 phase range to compensate for the phase delays at different positions on the antenna aperture so that the antenna can convert the incident field phase front from spherical to the plane phase front. As the holographic technique reduces the required phase range, it reduces the number of layers and air gaps used in the cell's structure. Furthermore, it allows using metasurfaces, which improves antenna bandwidth and radiation efficiency.

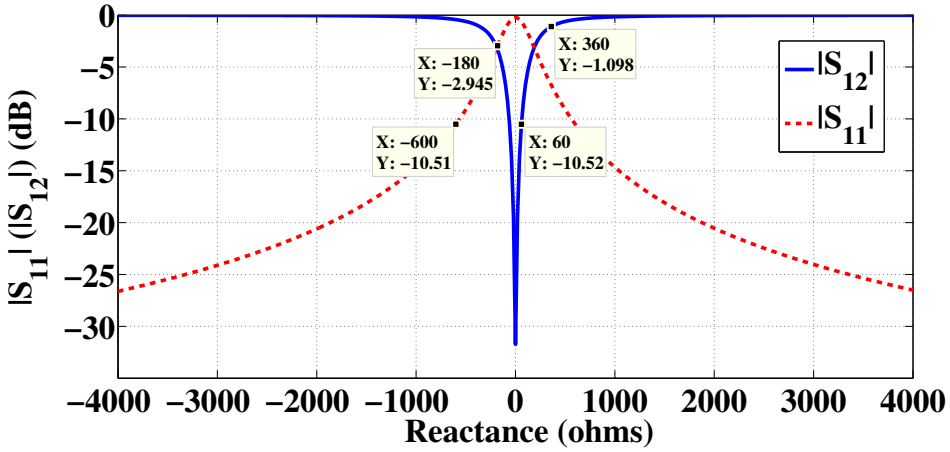

Figure 1. Transmission (reflection) magnitudes as a function of the impedance values. Note that the sheet is a square patch with a length of 4 mm, and the simulation frequency is 15 GHz.

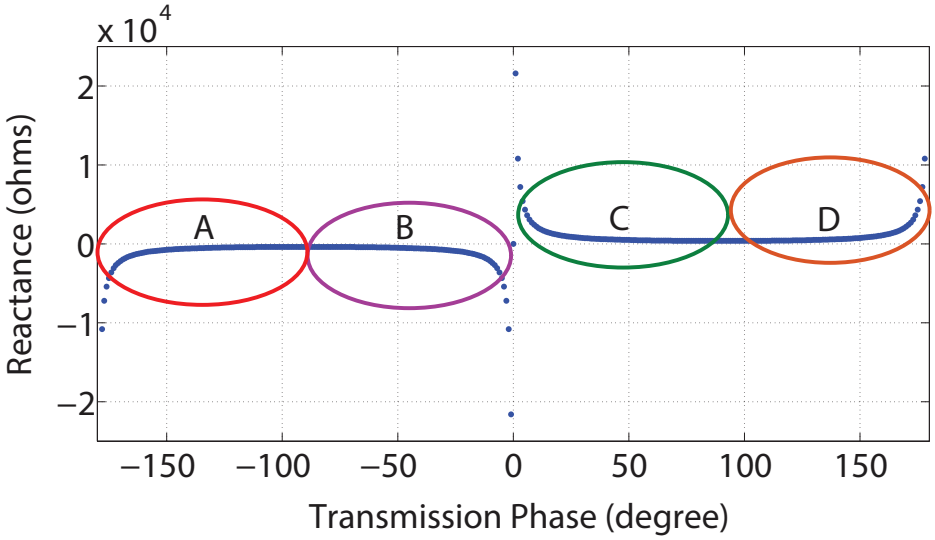

Figure 2. The transmission reactance values in terms of the transmission phase under the following assumptions: lossless unit cell ($\left|S_{11}\right| = 0, \left|S_{12}\right| = 1$), and available phase range $= 360^0$ Apparently, A=B , and C=D.

Holographic Transmitarray Description

The following steps summarize the procedure of designing a holographic transmitarray: 1- designing the mathematical hologram and sampling it with a sampling rate associated with the cell periodicity to obtain the interferogram 2- Implementing the impedance (admittance) description of the hologram by using quasi-periodic unit cells. The mathematical hologram is obtained from Eq.(5). For a linear space feed holographic transmitarray antenna, the reference wave is a spherical wave emitted by the horn antenna, and the object wave is a plane wave with a directed beam at (θ_0,ϕ_0), as defined in Eq.(6) and Eq.(7), where $\hat{r}_i = x_i\hat{x} + y_i\hat{y} + z_i\hat{i}$ and $\hat{r}_o = (x_i \sin(\theta_0)\cos(\phi_0) + y_i \sin(\theta_0)\cos(\phi_0) + z_i \cos(\phi_0))$. By substituting Eq.(6) and Eq.(7) in Eq.(5), the mathematical hologram is obtained in Eq.(8). Note that (x_f,y_f,H) designates for the feed position.

$$\psi_{obj}(x_i, y_i) = e^{-jk_0(\hat{r}_i \cdot \hat{r}_o)} = e^{-jk_0(x_i \sin(\theta_0)\cos(\phi_0) + y_i \sin(\theta_0)\sin(\phi_0) + z_i \cos(\phi_0)} \Big| z_i = 0 \tag{6}$$

$$\psi_{ref}(x_i, y_i) = e^{-jk_0 r} = e^{-jk_0 r} = e^{-jk_0\sqrt{(y_i - y_f)^2 + (x_i - x_f)^+ H^2}} \tag{7}$$

$$Z(x,y)|Y(x,y) = j\left(X + M\left(\cos\left(k_0(r - x_i \sin(\theta_0)\cos(\phi_0) - y_i \sin(\theta_0)\sin(\phi_0))\right)\right)\right) \tag{8}$$

Eq.(5) is a modulated cosine function. As the cosine function generates positive, negative, and zero values, Eq.(4) always generate reactance values between ± 360 ohms. However, according to Fig.2, a transmission artificial impedance surface cannot generate such reactance values while experiencing transmission magnitudes better than -1 dB. Therefore, Eq.(8) cannot be implemented as a holographic TA. However, it can be implemented as a holographic RA, similar to holographic RAs proposed in [2,3,5]. We dub this impedance zone 'holographic reflectarray antenna zone (HRAZ)' or 'holographic transmitarray forbidden zone (HTAFZ).' Here, a solution is proposed to avoid HTAFZ. First, Eq.(8) is converted to two equations by creating two conditions. Second, two arbitrary constants are added to these equations. Because X is the arbitrary average impedance (admittance) value and does not contain the amplitude and phase information of the object waves, we are allowed to change it. The new impedance (admittance) description of the hologram is given by Eq.(9):

$$\begin{cases} Z_{new}|Y_{new} = Z_{old}|Y_{old} + A & if(Z_{old}|Y_{old}<0) \\ Z_{new}|Y_{new} = Z_{old}|Y_{old} + B & if(Z_{old}|Y_{old}>0) \end{cases} \tag{9}$$

where A and B are the two arbitrary constants. By adequately determining these values, the hologram can pass the HTAFZ. The holographic technique can be applied to generate more than one object wave. In this case, the hologram records the information (phase and amplitude) of all object waves. The superposition of the object waves is expressed Eq.(10).

$$\psi_{obj}^{total} = \left(\sum_{i=1}^{i=n} \psi_o^i bj \right) \tag{10}$$

Unit Cell Design

A unit cell consisting of three identical layers of square ring elements and circular patch elements is employed, as seen in Fig.3a and Fig.3b. Variable radius length R (0.1 mm to 2.9 mm) with periodicity P=0.26λ_0=6.6 mm, and square ring width W=0.2 mm are considered. The elements are printed on a dielectric layer made by Rogers 4003C with thickness T= 0.508 mm and relative permittivity ($\varepsilon_r = 3.55$). The air gap height between every two layers equals H=0.24λ_0=6 mm. The equivalent circuit of every layer is shown in Fig.3c. The circular patch (shunt capacitor) creates a low-pass response while the square ring (shunt inductor) creates a high-pass response. These two elements create a band-pass response. The resistor represents losses due to the substrate thickness. The cell is simulated under the periodic boundary conditions using the CST Microwave Studio frequency-domain solver at 12 GHz. Simulation results are presented in Fig.4a up to Fig.4d. According to Fig.4a, for the normal incident angle, transmission magnitudes better than -1 dB are obtained by varying the radius length from 0.1 mm to 2.85 mm while, for the incident angle of $\theta = 30$, this criterion is achieved by varying radius length from 1.5 mm to 2.9 mm. As seen in Fig.4b, the unit cell provides (232^0) phase shifts when it is illuminated under the normal incident angle while it allows for (242^0) phase shifts when it is illuminated under the incident angle of($\theta = 30^0$).

The transmission susceptance and resistance values are presented in Fig.4c and Fig.4d, respectively, for incident angles of $\theta = 0^0$ and $\theta = 30^0$. According to the figures, the susceptance curves have resonance points where the resistance values increase or decrease sharply, indicating some losses. Therefore, it is necessary to eliminate the resonance points from the available admittance range, as seen in Fig.5. Moreover, Fig.4a up to Fig.4d show that transmission coefficients change considerably by varying the incident angle. These discrepancies increase the sidelobe and backlobe level of the final antenna. Thus, the unit cell is simulated under various incident angles from 0^0 to 50^0, with step 5^0 to avoid the above disadvantages. It is worthwhile to mention that $|S_{12}|$ better than -1 dB is set as a criterion for all incident angles to avoid high backlobe level.

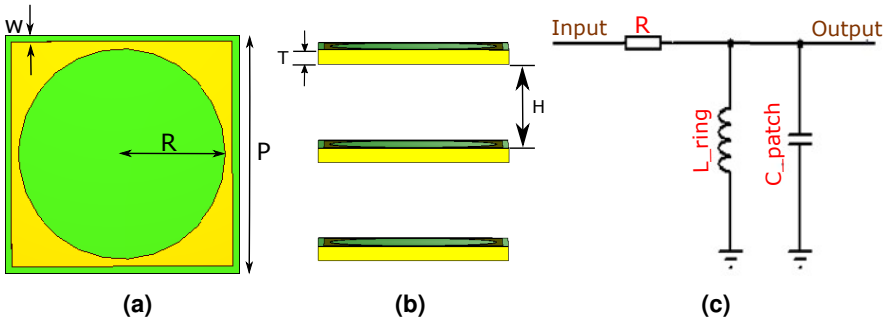

Figure 3. The triple layer unit-cell layout of a square ring element and a circular patch. (a) top view, (b) side view, and (c) the equivalent circuit of one layer unit-cell. Note that the green parts represent metal, and the yellow parts represent dielectric.

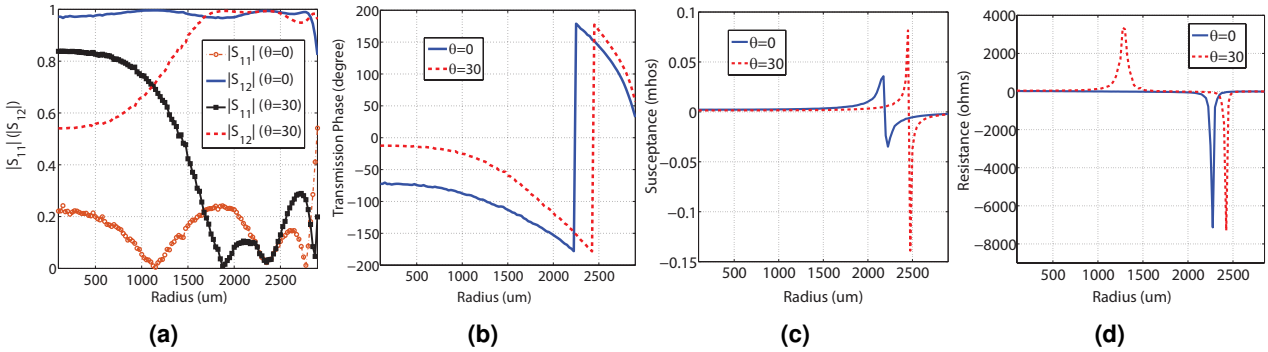

Figure 4. (a) Simulated transmission and reflection magnitudes in terms of the circular patch radius R under the incident angles of $\theta = 0$, and $\theta = 30$ at 12 GHz.(b) Simulated transmission phases in terms of the circular patch radius R under the incident angles of $\theta = 0$, and $\theta = 30$ at 12 GHz.(c) Simulated susceptance values in terms of the circular patch radius R under the incident angles of $\theta = 0$, and $\theta = 30$ at 12 GHz.(d) Simulated resistance values in terms of the circular patch radius R under the incident angles of $\theta = 0$, and $\theta = 30$ at 12 GHz.

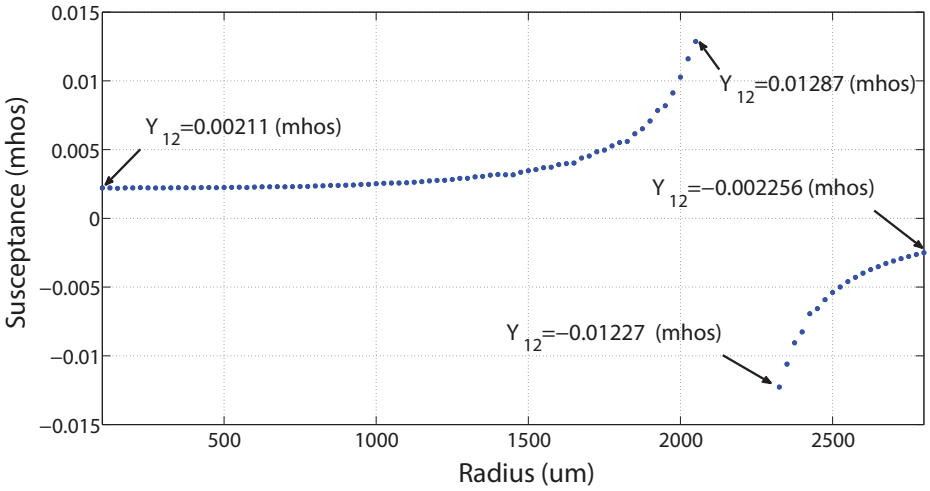

Figure 5. Simulated susceptance values in terms of the circular patch radius R under the normal incident angle at 12 GHz. The bounds are specified with arrows. The maximum susceptance value is 0.01287, and the minimum value equals -0.01227.

Hologram Design

In this section, several examples are provided to validate the solution proposed in section 4.

1.1 Design Consideration

The design frequency of all antennas is 12 GHz, making them a suitable candidate for X-band applications. Moreover, all antennas have a circular aperture with a radius of 13.2 cm. For the antenna feed, we have used the ATM-90-440-6 pyramidal horn antenna. The feed's radiation pattern is estimated by $\cos^q(\theta)$, where q=5.2. At 12 GHz, the feed gain is 13.3 dB, and its E-plane and H-plane 10-dB beamwidths are ±35.767 and ±38.5, respectively. F/D is chosen as 0.6589 to suppress unwanted backlobes and achieve suitable aperture efficiency, leading to edge tapering of -11.4 dB and the maximum achievable aperture efficiency of 64.49%. Besides, in all examples, parameters of Eq.(9) are assigned as follows: X= - 0.000041, M=0.009680, A=0.01287 and B=- 0.01227. Note that A and B (see Fig.5) are the maximum and minimum of the available susceptance range, respectively.

1.2 Simulation Results

Four examples are provided to validate the proposed solution. In the first to third examples, holographic TAs are designed to radiate a pencil beam directed at (0, 0), (30, 0), and (30, 45), respectively. In the last example, a holographic TA is designed to radiate two pencil beams directed at (30, 0) and (30, 180). The simulated results of the above examples are shown in Fig.6a up to Fig.6e. Expectantly, the main beam direction varies by changing the frequency. According to the examples, when the

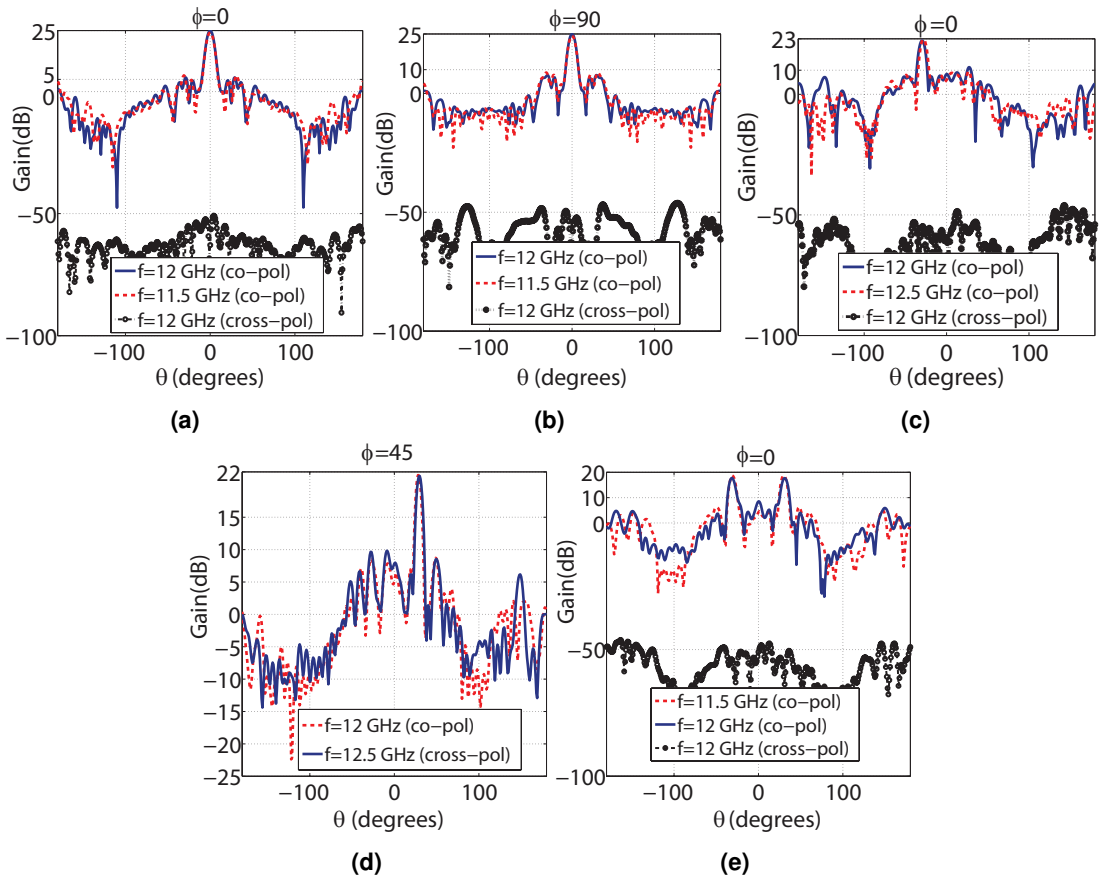

Figure 6. Simulated radiation pattern of the hologram. (a) Example 1 ($\phi = 0$) (b) Example 1 ($\phi = 90$), (c) Example 2, (d) Example 3,and (e) Example 4.

frequency shifts about 0.5 GHz from the center frequency (12 GHz), the main beam direction offsets about 2 degrees from θ_0. This causes reductions in the operating bandwidth of the proposed TAs. However, the beam squint can be ignored for the main lobe direction near to (0, 0). Generally, time-consuming iterative algorithms like PSO are used to synthesize array antenna based on the phase technique, while the above examples show that using the holographic technique leads to good results without the need of using time-consuming iterative algorithms. Furthermore, the cross-pol level is less than -50 dB for every examples.

Measurment Results

A holographic TA using the unit cell shown in Fig.3a, and Fig.3b is designed and manufactured. As the aperture efficiency of the square aperture antenna is lower than that of the circular one, a circular aperture holographic TA with a radius of 13.3 cm is fabricated, as seen in Fig.7a. The antenna feed is a pyramidal horn whose aperture size is $40 \times 26cm^2$. It operates at X band and uses the WR90 waveguide. The feed's gain is 12.5 dBi at 12 GHz, and its 10-dB beamwidths of E-plane and H-plane are ±37.33 and ±45.071, respectively. The feed radiation pattern is estimated with $\cos^{4.5}(\theta)$. The F/D ratio is selected as 0.659, according to the 10-dB beamwidths of the feed radiation pattern, leading to the maximum achievable aperture efficiency of 64.29%. Fig.7b shows the fabricated antenna and the measurement setup. The simulated and measured results are presented in Fig.8a and Fig.8b at E and H palnes. As seen in the figures, the measured maximum sidelobe level in $\phi = 0$ and $\phi = 90$ planes are 7.59 dB and 8.59 dB, respectively. Furthermore, the measured and simulated gains in terms of frequency are presented in Fig.9. Because of the phase center misalignment, fabrication errors corresponding to the feed horn and the array antenna, approximations of the simulation model, and antenna setting errors in the anechoic chamber, the measured gain is lower than the simulated gain. According to the figure, the simulated and measured 1-dB gain bandwidths are 13.3% (11.3 GHz-12.9 GHz) and 12.5% (11.4 GHz-12.9 GHz). The simulated and measured aperture efficiency at 12 GHz are 25.8% and 21.46%, respectively. Furthermore, the simulated radiation efficiency is 95.94%. Table 1 compares the proposed hologram with some existing works that are designed based on the only-phase technique. In terms of the 1-dB gain bandwidth, the proposed antenna performs better than [12-17]. This is mainly due to considering the effects of almost all incident angles on the transmission

admittance calculations and using subwavelength unit cells, which becomes possible due to using the holographic technique. In terms of the aperture efficiency, the performance of the hologram is better than[12]. However, it has worse performance than [13-17]. The reduction in the aperture efficiency is because of the low illumination and spillover efficiencies of the feed horn.

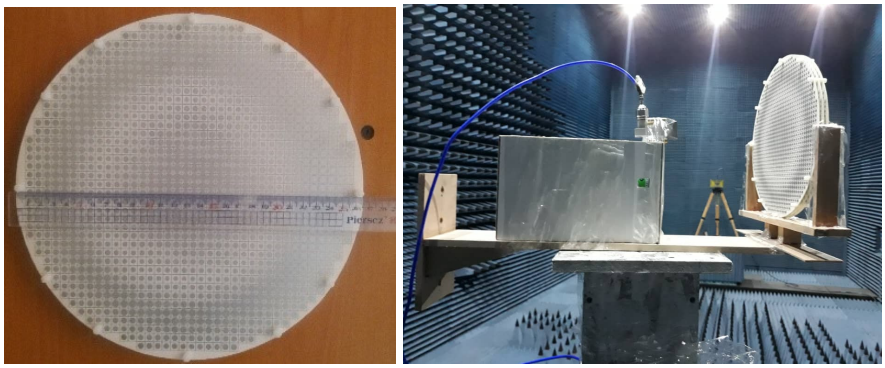

(a) (b)

Figure 7. (a) The manufactured transmitarray,and (b) The measurment setup.

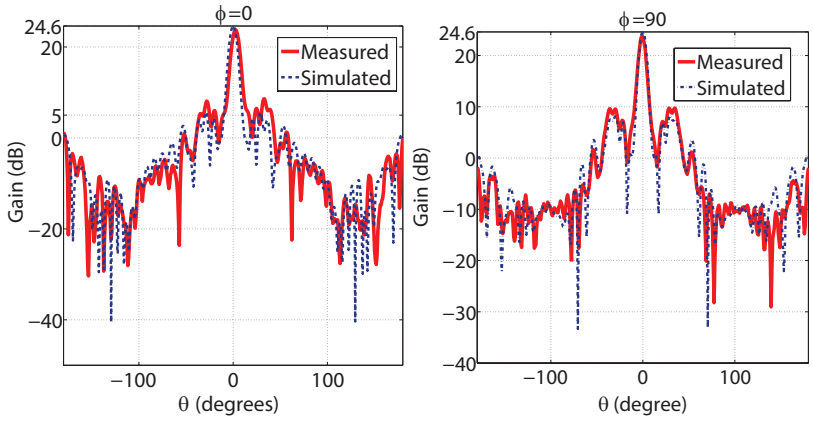

(a) (b)

Figure 8. The measured and simulated gains at 12 GHz. (a) yoz-plane, (b) xoz-plane.

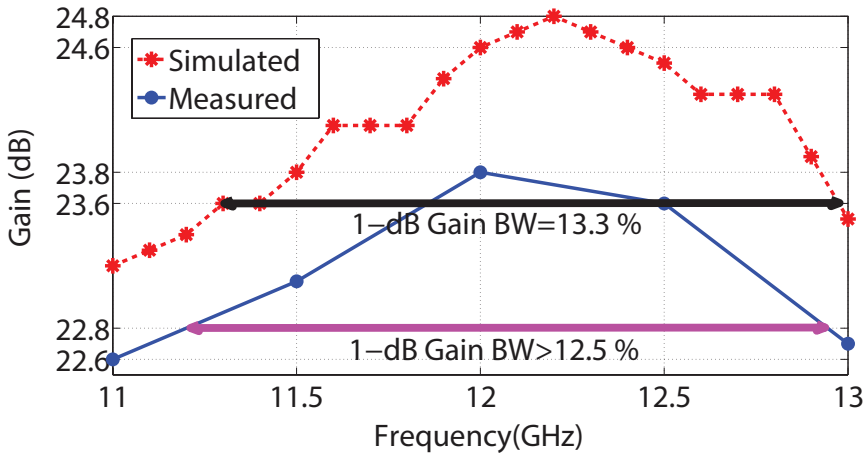

Figure 9. The measured and simulated gains versus frequency.

Ref	Freq (GHz)	Num.Layer	Metal-only	Gain (dB)	Aperture Efficiency (%)	1 dB Gian Bandwidth (%)
12	12.5	3	No	18.9	20.9	9.6
13	13.58	4	Yes	23.9	55	7.4
14	11.3	3	No	28.9	30	9
15	9.8	4	No	22.15	31	10.2
16	13.5	4	No	29.95	47	11.7
17	28.5	3	No	25	32.3	6.3
This Work	12	3	No	23.8	21.46	12.5

Table 1. Achievement comparison of our work with some existing TAs.

Conclusion

A detailed study on the design procedure of linearly polarized holographic transmitarrays for both the multi-beam and single-beam is presented for the first time. As the impedance values generated by an artificial impedance surface are different for the transmission and reflection states, a new approach based on the holographic technique is applied to record the amplitudes and phases of predetermined far-field radiations. Several examples are provided to support the proposed solution. Finally, a holographic TA is manufactured and tested. The simulation and measurement results show that the antenna has good performance in terms of the 1-dB gain bandwidth, mainly due to using elements with dimensions equal to $0.24\lambda_0$, which becomes possible due to the use of the holographic technique.

Author contributions statement

This project was done under the guidance of Prof. Oraizi as the supervisor. Mr. Salehi, as the primary author, proposed the method and performed the simulations. In doing so, he developed a Matlab code for synthesizing the holograms. He also analyzed the measurement and simulation results. All authors reviewed the manuscript.

Additional Information

Competing Interest: The authors declare no competing interests.

Data availability

Data availability: Data underlying the results presented in this paper are not publicly available at this time but may be obtained from the authors upon request.

References

1. F. Checcacci, V. Russo, and A. M. Scheggi, “Holographic antennas," *IEEE Transactions on Antennas and Propagation*, vol.18, Nov 1970.
2. Dawei Liu, Bo Cheng, Xiaotian Pan, Lifang Qiao, “A Horn-fed Frequency Scanning Holographic Antenna Based on Generalized Law of Reflection,"*SCIENTIFIC REPORTS*,12 August 2016.
3. Majid Karimipour, Nader Komjani, “Holographic-Inspired Multibeam Reflectarray with Linear Polarization," *IEEE Transactions on Antennas and Propagation*, vol.66, pp. 2870-2882, 12 June 2018.
4. Majid Karimipour, Nader Komjani, “Realization of Multiple Concurrent Beams with Independent Circular Polarizations by Holographic Reflectarray," *IEEE Transactions on Antennas and Propagation*, vol.66, pp.4627 - 4640, 13 June 2018.
5. Majid Karimipour, Nader Komjani, Iman Aryanian, “Shaping Electromagnetic Waves with Flexible and Continuous Control of the Beam Directions Using Holography and Convolution Theorem," *SCIENTIFIC REPORTS*,14 August 2019.
6. Shan Shan Gao, Hui Min Qiao and Jin Lin Li, “High Gain Holographic Antenna for Terahertz Applications," *Optical Materials Express*, Vol. 8, No. 2, 1 Feb 2018.
7. H. Oraizi, A. Amini, A. Abdolali and A. M. Karimimehr, “ Design of Wideband Leaky wave Antenna using Sinusoidally Modulated Impedance Surface Based on The Holographi Theory ," *Antennas and Wireless Propagation Letters*, vol. 17, pp. 1807-1811, 22 August 2018.
8. Mohammad Moein Moeini, Homayoon Oraizi, Amrollah Amini, Vahid Nayyeri, “Wide-band Beam-scanning by Surface Wave Confinement on Leaky wave Holograms ," *SCIENTIFIC REPORTS*, 13 September 2019.

9. Hedieh Emamian, Homayoon Oraizi, Mohammad Moein Moieni, “Design of Wide-band Dual-beam Leaky wave Antenna using the Holographic Theory," *27th Iranian Conference on Electrical Engineering*, 5 August 2019.

10. Gabrielle Minatti, Francesco Caminita, Massimilano Casaletti and Stefano Maci, “Spiral Leaky wave Antennas Based on Modulated Surface Imnpedance," *IEEE Transactions on Antennas and Propagation*, vol 59, pp 4436-4444, 22 August 2011.

11. M. Chen, “ Manipulating antenna radiation with angle holography,"*M.S. thesis*, Dept. Electron. Eng, Toronto, Univ., Toronto, Canada, 2015.

12. Jianfeng Yu, Lei Chen, Jing Yang and Xiaowei Shi , “Design of a Transmitarray Using Split Diagonal Cross Elements with Limited phase Range,"*IEEE Antennas and Wireless Propagation Letters*, VOL. 15, pp. 1514-1517,12 January 2016.

13. Guang Liu, Hong-jian Wang, Jing-shan Jiang, Fei Xue, and Min Yi, “A High-Efficiency Transmitarray Antenna Using Double Split Ring Slot Elements,"*IEEE Antennas and Wireless Propagation Letters*, VOL. 14, pp. 1415-1418, 6 March 2015.

14. Ahmed H. Abdelrahman, Payam Nayeri, Atef Z. Elsherbeni, and Fan Yang, “High-Gain and Broadband Transmitarray Antenna Using Triple-Layer Spiral Dipole Elements,"*IEEE Antennas and Wireless Propagation Letters*, VOL. 13, pp. 1288-1291, 2 July 2014.

15. Chao Tian, Yong-Chang Jiao and Gang Zhao, “A Wideband Transmitarray using Double-Petal Loop Elements," *Progress In Electromagnetics Research Letters*, Vol. 59, pp. 57–62, 2016.

16. Ahmed H. Abdelrahman, Payam Nayeri, Atef Z. Elsherbeni, and Fan Yang, “Bandwidth Improvement Methods of Transmitarray Antennas,"*IEEE Transactions on Antennas and Propagation Letters*, vol.63, no.7,pp.2946-2954,7 July 2015.

17. Guang Liu, Mohammad Reza Dehghani Kodnoeih, Kien T. Pham, Eduardo Motta Cruz, David González-Ovejero, and Ronan Sauleau, “A Millimeter Wave Multi-beam Transparent Transmitarray Antenna at Ka-band,"*IEEE Antennas and Wireless Propagation Letters*, VOL. 18, pp. 631-635, 18 February 2019.

Figures

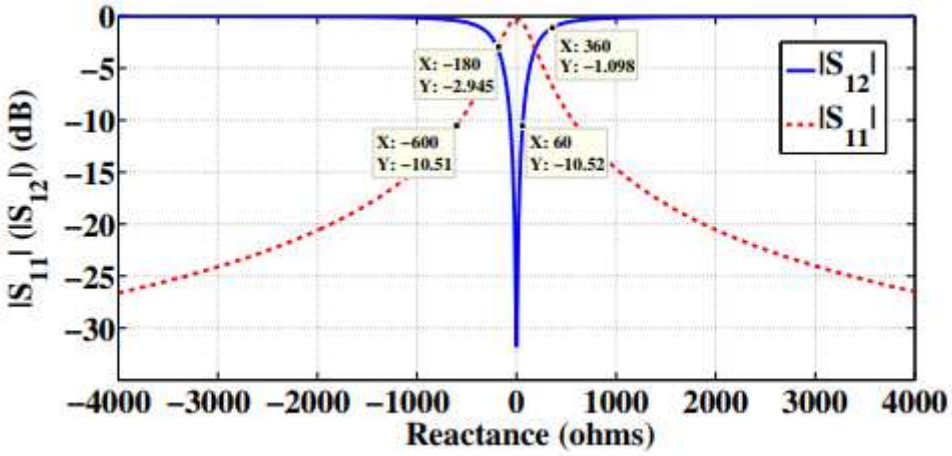

Figure 1

Transmission (reflection) magnitudes as a function of the impedance values. Note that the sheet is a square patch with a length of 4 mm, and the simulation frequency is 15 GHz.

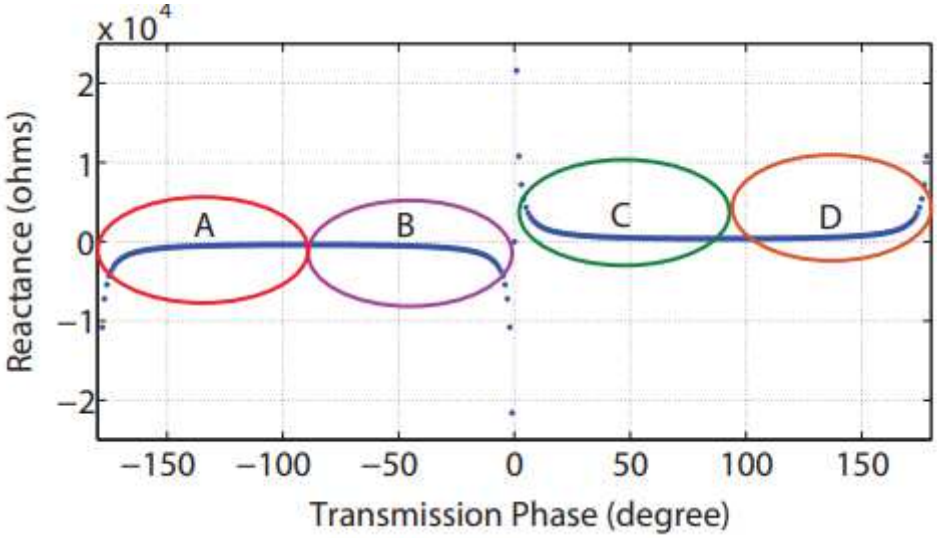

Figure 2

[Please see the manuscript file to view this figure caption.]

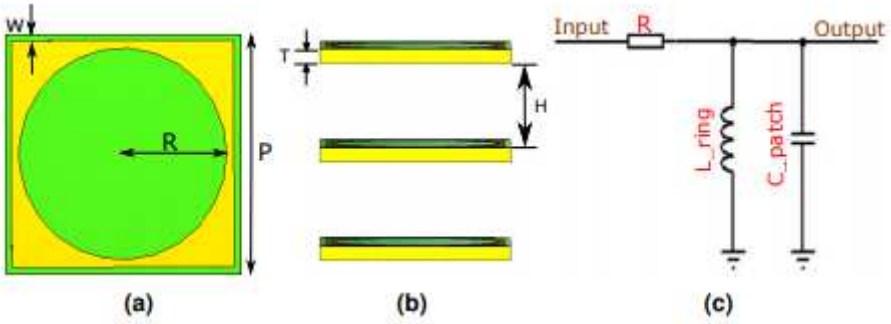

Figure 3

The triple layer unit-cell layout of a square ring element and a circular patch. (a) top view, (b) side view, and (c) the equivalent circuit of one layer unit-cell. Note that the green parts represent metal, and the yellow parts represent dielectric.

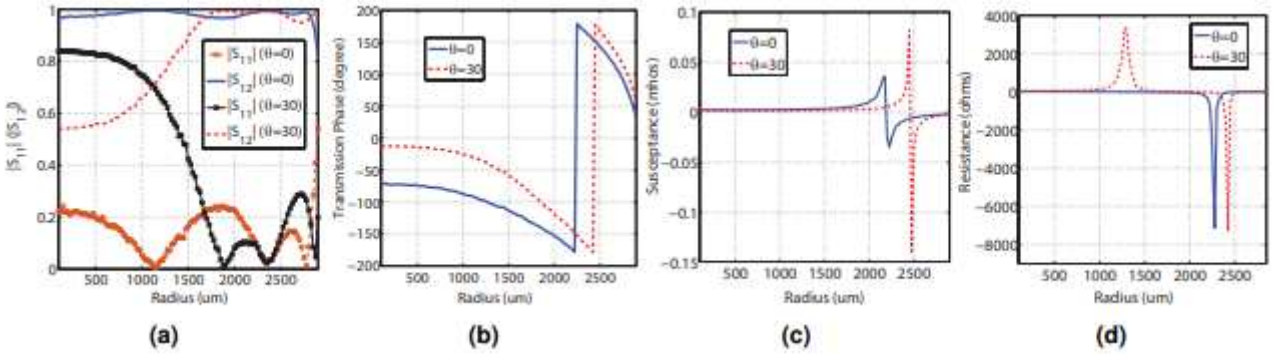

Figure 4

(a) Simulated transmission and reflection magnitudes in terms of the circular patch radius R under the incident angles of θ = 0, and θ = 30 at 12 GHz.(b) Simulated transmission phases in terms of the circular patch radius R under the incident angles of θ = 0, and θ = 30 at 12 GHz.(c) Simulated susceptance values in terms of the circular patch radius R under the incident angles of θ = 0, and θ = 30 at 12 GHz.(d) Simulated resistance values in terms of the circular patch radius R under the incident angles of θ = 0, and θ = 30 at 12 GHz.

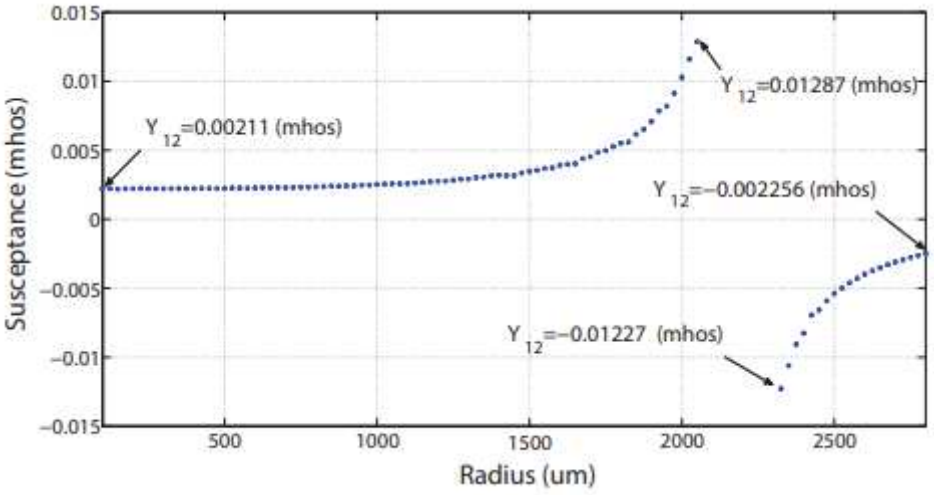

Figure 5

Simulated susceptance values in terms of the circular patch radius R under the normal incident angle at 12 GHz. The bounds are specified with arrows. The maximum susceptance value is 0.01287, and the minimum value equals -0.01227.

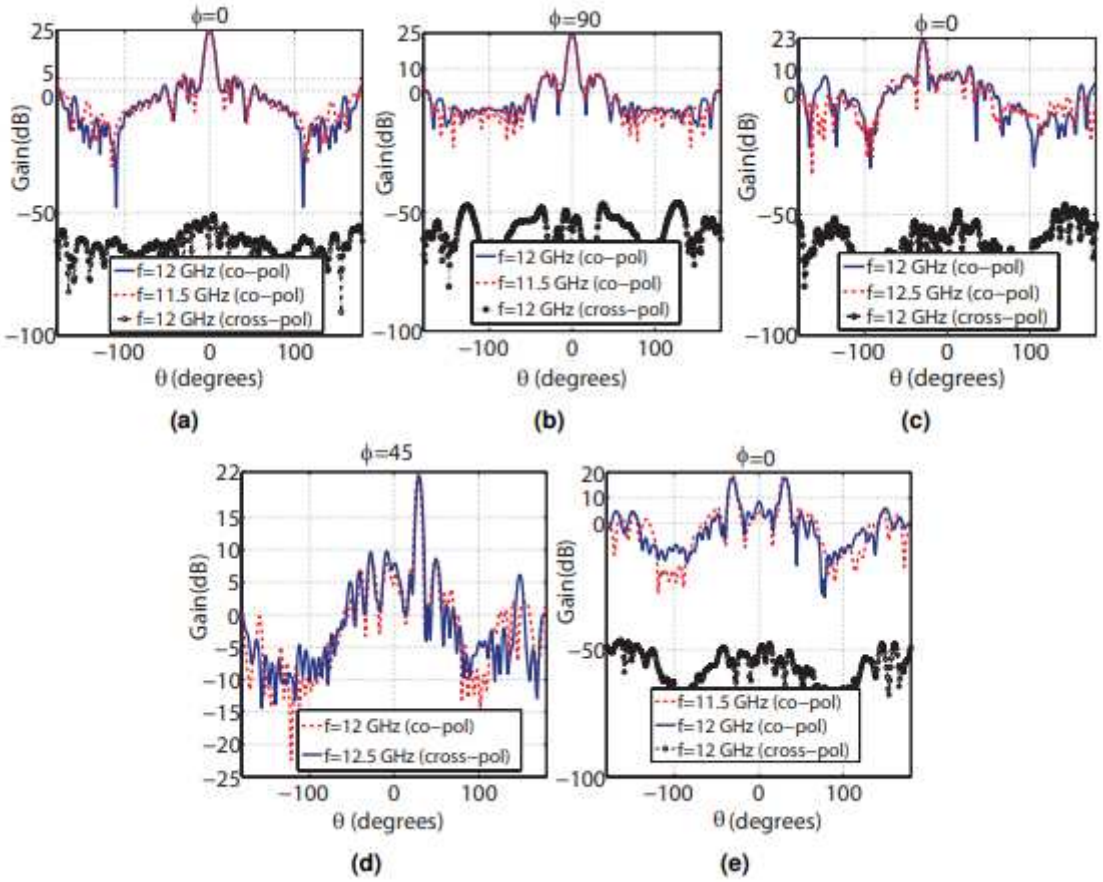

Figure 6

Simulated radiation pattern of the hologram. (a) Example 1 (φ = 0) (b) Example 1 (φ = 90), (c) Example 2, (d) Example 3,and (e) Example 4.

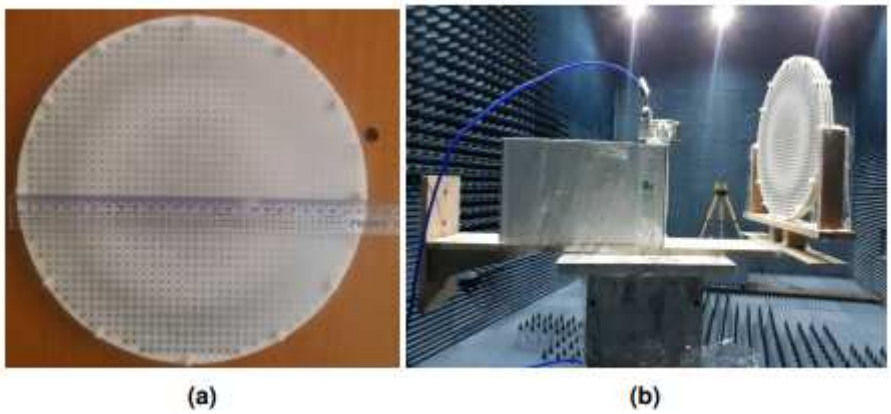

Figure 7

(a) The manufactured transmitarray,and (b) The measurment setup.

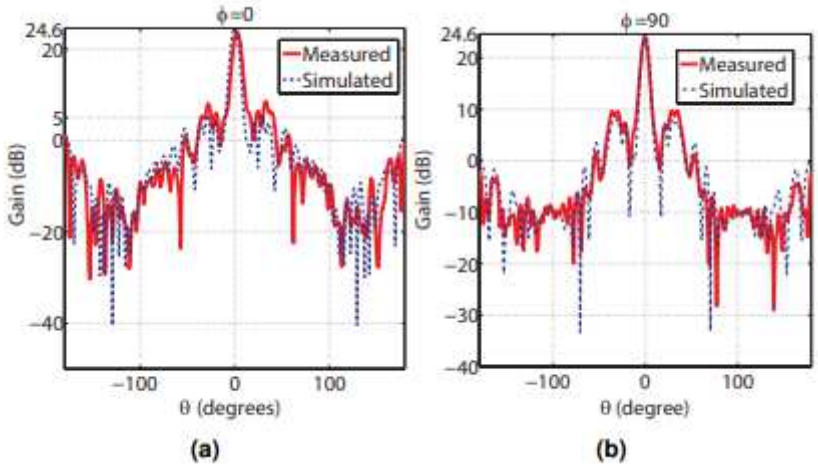

Figure 8

The measured and simulated gains at 12 GHz. (a) yoz-plane, (b) xoz-plane.

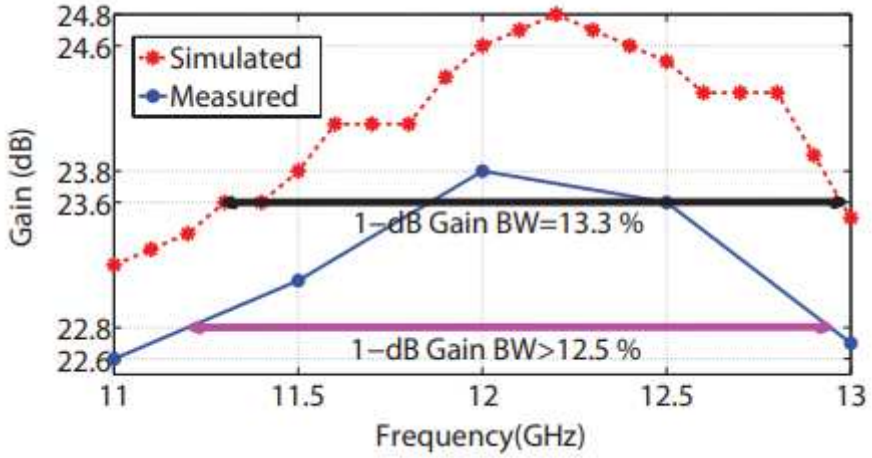

Figure 9

The measured and simulated gains versus frequency.